


Cite this: *RSC Adv.*, 2018, 8, 21664

Spitzer shaped ZnO nanostructures for enhancement of field electron emission behaviors

Parameshwar R. Chikate,^a Prashant K. Bankar,^b Ram J. Choudhary,^c Yuan-Ron Ma,^d Shankar I. Patil,^b Mahendra A. More,^b Deodatta M. Phase,^c Parasharam M. Shirage^a and Rupesh S. Devan^{*,a}

We observed enhanced field emission (FE) behavior for spitzer shaped ZnO nanowires synthesized via a hydrothermal approach. The spitzer shaped and pointed tipped 1D ZnO nanowires of average diameter 120 nm and length ~5–6 μm were randomly grown over an ITO coated glass substrate. The turn-on field (E_{on}) of 1.56 $\text{V } \mu\text{m}^{-1}$ required to draw a current density of 10 $\mu\text{A cm}^{-2}$ from these spitzer shaped ZnO nanowires is significantly lower than that of pristine and doped ZnO nanostructures, and $\text{MoS}_2/\text{TiO}_2$ heterostructure based FE devices. The orthodoxy test that was performed confirms the feasibility of a field enhancement factor (β_{FE}) of 3924 for ZnO/ITO emitters. The enhancement in FE behavior can be attributed to the spitzer shaped nanotips, sharply pointed nanotips and individual dispersion of the ZnO nanowires. The ZnO/ITO emitters exhibited very stable electron emission with average current fluctuations of $\pm 5\%$. Our investigations suggest that the spitzer shaped ZnO nanowires have potential for further improving in electron emission and other functionalities after forming tunable nano-hetero-architectures with metal or conducting materials.

Received 17th April 2018

Accepted 25th May 2018

DOI: 10.1039/c8ra03282c

rsc.li/rsc-advances

Introduction

Among the various 1D nanostructure morphologies, nanowires and nanorods, offering the advantages of large surface areas, are found apposite to improve field electron emission. Carbon nanotubes are of great interest to field emission (FE) in particular because of their high aspect ratio, better electrical and thermal conductivity, and robust mechanical and chemical stability. However, the difficulties of establishing density controlled vertical nanotube growth at a lower cost have significantly impeded the practical execution of carbon nanotubes in field emission devices. Wide bandgap transition metal oxides such as NbO_2 , TiO_2 , CuO and SnO are known for their stability and are found to be suitable for field emission in their 1D forms such as wires, rods, tubes, needles *etc.*^{1–4} Even though ZnO is an attractive material for diverse applications in solar cells, catalysis, sensing, photocatalysis, smart windows, photoluminescence, supercapacitors, generators *etc.*, and is even more suitable for ultraviolet light emitters and laser diodes,^{4,5} it has only been moderately considered for use in FE displays

because of its larger work function in the range of 5.3 to 5.6 eV, limited morphological forms and field screening effect from uncontrolled dispersion.^{6–9} Therefore, emerging approaches to tailor the work function and improve electron emission such as the modification of emitter geometry, the introduction of impurity, decoration of metals and the vertical alignment of the structures have been reported.^{2,10} The implantation of elements into ZnO nanowires was found to produce nanoscale protruberances and surface-related defects which reduced the turn-on field (E_{on}) from 3.1 to 2.4 $\text{V } \mu\text{m}^{-1}$ (at 0.1 $\mu\text{A cm}^{-2}$).¹¹ However, Cu doping in ZnO *via* direct current magnetron sputtering in an Ar and O_2 environment deteriorated the crystalline quality by reducing the number of Zn interstitials and formed electron traps, which weakened the field emission and hence led to an E_{on} of 9 to 22.5 $\text{V } \mu\text{m}^{-1}$.¹² Despite the fact that doping of elements like Ga,¹³ Al,¹⁴ Mg,¹⁵ C,¹⁶ In¹⁷ *etc.* resulted in a favorable alteration of the electronic properties of ZnO which might have assisted in the lower possible E_{on} values of 2.4, 2.8, 5.99, 18 and 193 $\text{V } \mu\text{m}^{-1}$, respectively, for field emission, one cannot neglect that these values are defined at a lower current density ranging from 0.1 to 1 $\mu\text{A cm}^{-2}$.

The modification of critical surface bond length in the nano-regime can tailor the ZnO nanostructure morphologies of the pyramid-, pencil-, rod-, wire-, *etc.*, forms.¹⁸ However, metals were employed as catalysts in the growth process for control over the random alignment and density of the structures, which unfavorably tailored the field emission properties. The density controlled growth of ZnO nanopillars using self-assembled Ag

^aDiscipline of Metallurgy Engineering and Materials Science, Indian Institute of Technology Indore, Simrol, Indore 453552, India. E-mail: rupesh@iiti.ac.in; devan_rs@yahoo.co.in

^bDepartment of Physics, Savitribai Phule Pune University (Formerly, University of Pune), Pune 411007, India

^cUGC-DAE Consortium for Scientific Research, Khandwa Road, Indore 452001, India

^dDepartment of Physics, National Dong Hwa University, Hualien 97401, Taiwan, Republic of China



nano-islands/layers resulted in an E_{on} of $2.39 \text{ V } \mu\text{m}^{-1}$.¹⁹ Catalysts guided the vertical alignment of the ZnO nanowires on an insulating substrate such as sapphire which limited their application in photonic/electronic devices like field emitters.²⁰ On the other hand, it has been demonstrated that the needle morphological forms can emit electrons more easily.²¹ Many growth methods have been utilized to explore various 1D morphologies⁴ but the very few which are known to provide tip features are cursed with post-treatments such as annealing or *in situ* heating. The air annealed tip-morphology of ZnO nanorods exhibited an E_{on} of $3.5 \text{ V } \mu\text{m}^{-1}$ owing to its large rod-body diameter and shortened tips.²¹ C-Axis oriented ZnO nanorods *in situ* heated at 580°C in an O_2 atmosphere to grow on a Si substrate had an E_{on} of $2.57 \text{ V } \mu\text{m}^{-1}$ defined at a very low current density of $0.1 \text{ } \mu\text{A cm}^{-2}$.²² Zhao *et al.*²³ thermally annealed ZnO nanorods in oxygen, air and NH_3 to improve the E_{on} (at $0.1 \text{ } \mu\text{A cm}^{-2}$) from $8.8 \text{ V } \mu\text{m}^{-1}$ to $4.1 \text{ V } \mu\text{m}^{-1}$. Ghosh *et al.*²⁴ observed an enhancement in FE performance after capping the tips of randomly oriented and highly oxygen defective ZnO nanostructures with metal nanoparticles despite their larger values of work function (*i.e.* $5.04\text{--}4.7 \text{ eV}$). Therefore, for promising field emission performance, efforts on size reduction, uniform morphology, sharp tip features and periodic growth of pristine ZnO nanowires appears to be of scientific and technological importance.

In this work, we present the synthesis of large-area arrays of randomly oriented spitzer shaped truncated/pointed ZnO nanowires grown periodically like Christmas trees using hydrothermal methods as excellent field emitters. The influence of the spitzer shaped tip morphologies of the 1D ZnO nanowires on field electron emission properties was studied methodically. The surface morphological features, and chemical and electronic structure of pristine ZnO nanowires were revealed using field-emission scanning electron microscopy (FESEM) and X-ray photoelectron spectroscopy (XPS). The FE behaviors of pristine 1D ZnO nanowires were studied at optimized anode–cathode separation and it was observed that at a separation of $2000 \text{ } \mu\text{m}$ the 1D spitzer shaped hexagonal ZnO nanowires exhibited excellent FE properties.

Experimental

Large area arrays of ZnO nanowires were synthesized on ITO coated glass substrates *via* a hydrothermal approach. Zinc acetate dihydrate ($\text{C}_4\text{H}_6\text{O}_4\text{Zn} \cdot 2\text{H}_2\text{O}$, 98%, Sigma Aldrich) and sodium peroxide (Na_2O_2 , 97%, Sigma Aldrich) at 30 mM L^{-1} and 100 mM L^{-1} concentrations, respectively, were mixed to form a 1 : 1 solution. This solution was stirred at room temperature for 30 min and then transferred to an autoclave containing well aligned ITO coated glass substrates. The hydrothermal reaction was carried out at 85°C for 12 h to grow 1D ZnO nanowires over the ITO coated glass substrate. After that, the surface morphology of the pristine ZnO nanowires was confirmed using field emission scanning electron microscopy (FESEM, Carl Zeiss, Merlin 6073). The chemical states of the ZnO nanowires were analyzed using an X-ray photoelectron spectrometer (XPS, Thermo Scientific Inc. K_α) with a microfocus monochromated

Al K_α X-ray. The valence band spectra (VBS) were measured using an Omicron energy analyzer (EA-125, Germany) with an angle incidence photo-emission spectroscopy (AIPES) beamline on an Indus-1 synchrotron source at RRCAT, Indore, India. The FE studies of the pristine ZnO nanowires were carried out in a vacuum chamber maintained at a base pressure of $\sim 7.5 \times 10^{-9} \text{ Torr}$. The anode semi-transparent phosphor screen was maintained at various distances of 1500, 2000 and $2500 \text{ } \mu\text{m}$ from the pristine ZnO nanowires ($\equiv \text{ZnO/ITO}$ emitter). Samples were preconditioned at a voltage of $\sim 3 \text{ kV}$ for 30 min to avoid the influence of contamination and loosely bound nanowires in the field emission. The field emission current (I) was measured with an electrometer (Keithley 6514) at a direct current (dc) voltage (V) applied using a high-voltage dc power supply ($0\text{--}40 \text{ kV}$, Spellman). The long-term stability of the field emission current was recorded for the ZnO/ITO emitters.

Results and discussion

The FESEM images in Fig. 1 show the surface morphology of large area arrays of ZnO nanowires grown over ITO coated conducting glass substrates. The hexagonal ZnO nanowires are confined to a limited range of diameter ($<180 \text{ nm}$). The well-separated nanowires with clearly visible textural boundaries were of an average body diameter of $\sim 120 \text{ nm}$ and were $\sim 5\text{--}6 \text{ } \mu\text{m}$ long (Fig. 1(a)). These distinct ZnO nanowires were well arranged in the form of Christmas trees which appeared like a forest of well separated and periodically arranged trees, (Fig. 1(a)), to deliver highly porous thin films of thickness $\sim 1300 \text{ nm}$ (Fig. 1(b)). Close examination of the ZnO nanowire array revealed the curtailing of the hexagonal facets at its tip, which resulted in the formation of spitzer shaped truncated/pointed tips (Fig. 1(c)). The spitzer shaped ZnO nanowires with truncated tips at the top of the trees had diameters less than $\sim 30 \text{ nm}$ (Fig. 1(c)). The spitzer shaped truncated tip construction of ZnO nanowires is expected to govern the enhanced FE behaviors. The electronic structure and chemical properties of spitzer shaped ZnO nanowires were confirmed by XPS investigations. Fig. 2 shows the high-resolution XPS spectra of the Zn(2p) core level of the ZnO nanowires. The clearly observable double peak feature of Zn($2p_{3/2}$) and Zn($2p_{1/2}$) located at a binding energy of $1020.9 (\pm 0.1)$ and $1044.0 (\pm 0.1) \text{ eV}$, respectively, represents the core level of Zn^{2+} cations.^{5,25} The estimated energy separation of 23.1 eV , assigned to ZnO and not metallic Zn,²⁶ was maintained between the Zn(2p) core levels of the spitzer shaped nanowires.

The FE measurements of the spitzer shaped 1D ZnO nanowires ($\equiv 1\text{D ZnO/ITO}$) were performed in the planar diode configuration. The emitting device with an emission area of $\sim 0.30 \text{ cm}^2$ was maintained with anode–cathode separations of 1500, 2000 and $2500 \text{ } \mu\text{m}$. The applied electric field (E) dependent variation in the electron emission current density (J) (*i.e.* $J\text{--}E$ plot) of the ZnO/ITO emitters is shown in Fig. 3(a). Although spitzer shaped ZnO nanowires are periodically arranged in the form of trees, their random orientation leads to the applied electric field ($E = V/d_{\text{sep}}$) being treated as the average field and not the uniform field between the electrodes separated by the



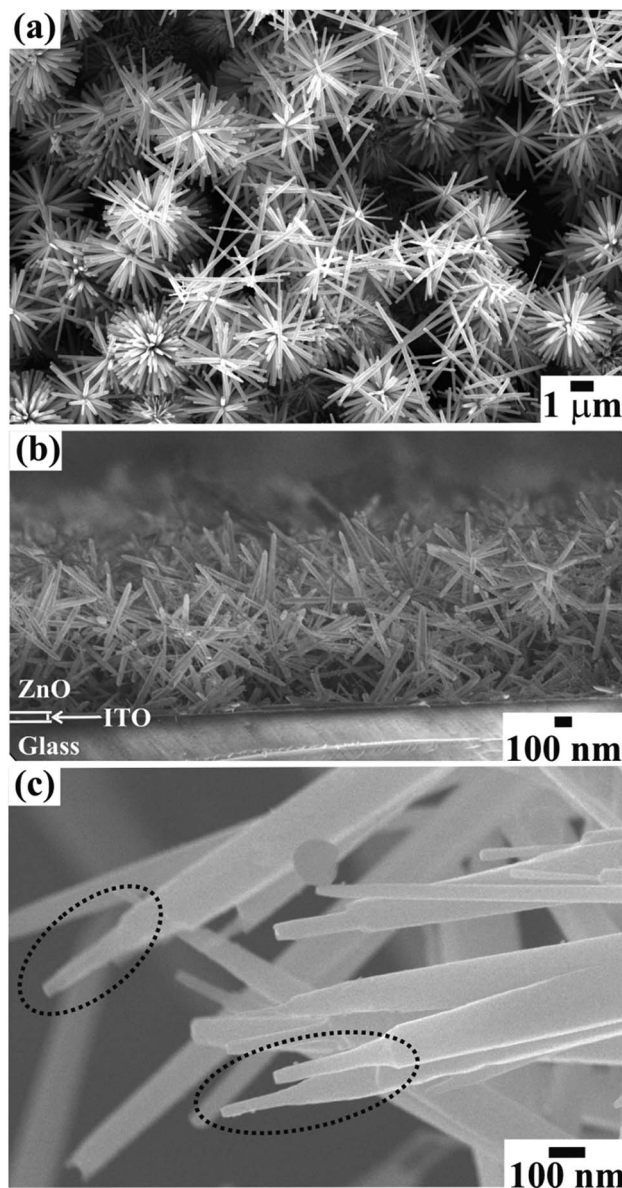


Fig. 1 FESEM images showing the (a) top view and (b) side view of a large area array of ZnO nanowires with (c) spitzer shaped morphologies grown on ITO coated glass substrate.

distance d_{sep} . The spitzer shaped ZnO nanowires ($\equiv \text{ZnO/ITO}$) were subjected to electron field emission at separations of 1500, 2000 and 2500 μm to confirm the optimized field emission behavior. The large emission current density of $572 \mu\text{A cm}^{-2}$, lower threshold field (E_{thr}) of $1.9 \text{ V } \mu\text{m}^{-1}$ and lower E_{on} of $1.56 \text{ V } \mu\text{m}^{-1}$ were observed at 2000 μm . However, the lowest E_{on} ($1.16 \text{ V } \mu\text{m}^{-1}$) was observed at the separation of 2500 μm with the emission current density decreased significantly to $198 \mu\text{A cm}^{-2}$. The E_{on} observed for these spitzer shaped truncated tip ZnO nanowire arrays is much lower than that reported for ZnO nanorods grown on Si substrates using PLD (*i.e.* $2 \text{ V } \mu\text{m}^{-1}$),⁶ ZnO nanopillars grown by vapor transport deposition (*i.e.* $3.15 \text{ V } \mu\text{m}^{-1}$),²⁷ ZnO nanorods and nanodisk networks (*i.e.* 4.8 and $2.6 \text{ V } \mu\text{m}^{-1}$, respectively, reported at $1 \mu\text{A cm}^{-2}$),⁷ ZnO

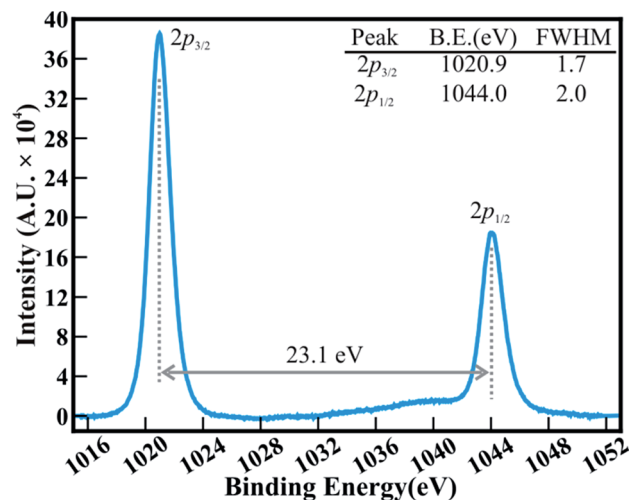


Fig. 2 High-resolution XPS spectra of the Zn(2p) core levels of spitzer shaped ZnO nanowires.

nanoneedles (*i.e.* $2.4 \text{ V } \mu\text{m}^{-1}$) and bottle-like nanorods (*i.e.* $4.6 \text{ V } \mu\text{m}^{-1}$) fabricated using vapor phase growth,⁸ ZnO agave-like (*i.e.* $2.4 \text{ V } \mu\text{m}^{-1}$) and pencil-like (*i.e.* $3.7 \text{ V } \mu\text{m}^{-1}$) nanostructures grown on amorphous carbon,⁹ nitrogen implanted ZnO nanowires (*i.e.* $2.4 \text{ V } \mu\text{m}^{-1}$ at a current density of $0.1 \mu\text{A cm}^{-2}$),¹¹ metal (Ag/Pt/Au) loaded ZnO nanorods (*i.e.* 1.9 and $2.6 \text{ V } \mu\text{m}^{-1}$, respectively),²⁸ CuO nanoplates (*i.e.*, $6.7 \text{ V } \mu\text{m}^{-1}$),³ ZnO nanotetrapods screen-printed on carbon nanofiber buffered Ag (*i.e.* $6.7 \text{ V } \mu\text{m}^{-1}$ defined at $0.1 \mu\text{A cm}^{-2}$)²⁹ and brookite TiO_2 .^{2,30} C-Axis oriented ZnO nanocones were expected to deliver better field emission because of the tapered cone-like morphology, nevertheless, the E_{on} obtained at a very low current density of $0.1 \mu\text{A cm}^{-2}$ was restricted to $2.57 \text{ V } \mu\text{m}^{-1}$ which might be due to the very low areal density of ZnO nanocones.²² Dense morphology reported as hexagonal flower-like ZnO nanowhiskers delivered an E_{on} of $2.2 \text{ V } \mu\text{m}^{-1}$ (at a current density of $0.1 \mu\text{A cm}^{-2}$) which might be due to the diameter of the whiskers being limited to 300 nm.³¹ The n-type nitrogen³² or H-plasma³³ treated ZnO nanowires were not successful at improving the E_{on} beyond $2.1 \text{ V } \mu\text{m}^{-1}$. Furthermore, Sugavaneshwar *et al.*³⁴ have reported an enhancement in the field emission of branched ZnO nanostructures compared to that of simpler nanostructures such as nanowires and nanorods, *etc.*, but the actual values of E_{on} were not stated. Although Chang *et al.*²⁷ have reported an enhancement in the FE properties of ZnO nanopillars after decorating Au nanoparticles along the surface, the minimum E_{on} of the ZnO nanopillars which was limited to $3.15 \text{ V } \mu\text{m}^{-1}$ was further reduced to $2.65 \text{ V } \mu\text{m}^{-1}$ (after Au decoration) owing to the larger diameter and flat top of the ZnO nanopillars (*i.e.* $\sim 200 \text{ nm}$). Additionally, the selective patterning of ZnO nanorods achieved an E_{on} of $2.85 \text{ V } \mu\text{m}^{-1}$.³⁵ The possible reasons behind such higher turn-on values are the flat tips, nonuniform morphologies, uneven distribution and larger diameter of the 1D ZnO structures. Moreover, the emission current density of $572 \mu\text{A cm}^{-2}$ attained at a lower applied field of $2.34 \text{ V } \mu\text{m}^{-1}$ for ZnO nanowires ($\equiv \text{ZnO/ITO}$) is



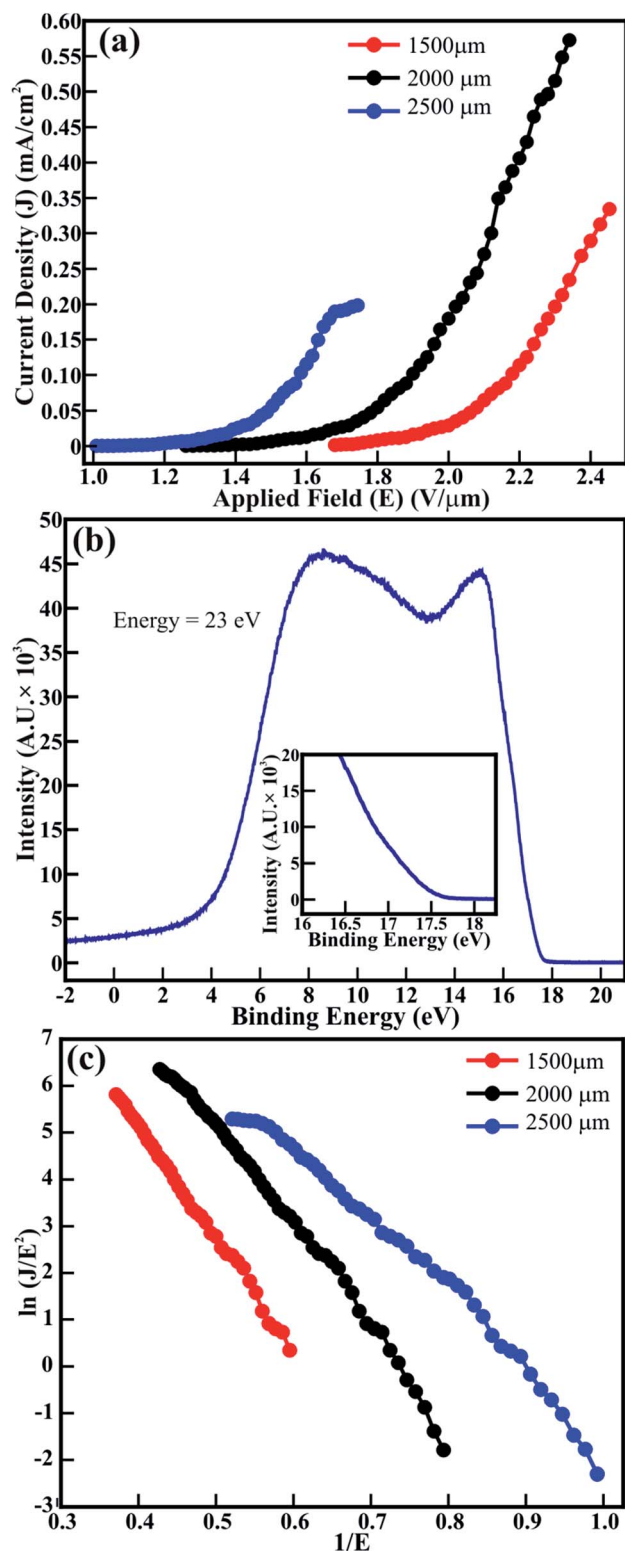


Fig. 3 Field emission (a) J - E curves and (c) F-N plots obtained from the J - E curves, and (b) UPS valence band spectra measured for spitzer shaped ZnO nanowires. The inset in (b) shows the magnified valence band spectra at the higher binding energy.

reasonably higher than that reported for pristine and Al (*i.e.* $\sim 4 \mu\text{A cm}^{-2}$ and $\sim 3 \mu\text{A cm}^{-2}$, respectively),¹⁴ C (*i.e.* $16 \mu\text{A cm}^{-2}$)¹⁶ and In (*i.e.* $1.5 \mu\text{A cm}^{-2}$)¹⁷ doped ZnO nanostructures.¹⁷ In

contrast, pristine ZnO and Mg-doped ZnO nanostructures have drawn slightly better emission currents (*i.e.* 0.8 to 3.2 mA cm^{-2}) at the much higher applied field of $9.2 \text{ V } \mu\text{m}^{-1}$.¹⁵

Reduction of the work function enhances FE properties. Therefore, ultraviolet photoelectron spectroscopy (UPS) was utilized to estimate the work function of ZnO/ITO emitters. The UPS spectra recorded for a ZnO nanowire array at an energy of 23 eV is shown in Fig. 3(b). Two distinct peaks in the VBS of ZnO nanowires located at higher and lower binding energies are assigned to the hybridization of the O(2p) and Zn(4s) orbitals, and nonbonding O(2p) orbitals respectively.³⁶ Moreover, the work functions of ZnO emitters are estimated from the equation³⁷

$$\Phi_{\text{ZnO}} = h\nu - |E_{\text{sec}} - E_{\text{FE}}| \quad (1)$$

where $h\nu$ is the energy of the source utilized ($\equiv 23 \text{ eV}$), E_{sec} is the onset of the secondary emission and E_{FE} is the Fermi edge. The spitzer shaped truncated tip appearance of the ZnO nanowires resulted in a lower work-function of 4.9 eV (*i.e.* Φ_{ZnO}) than that of reported ZnO nanostructures such as nanorods and nanowires,^{10,14} oxygen plasma treated ZnO (*i.e.* 5.5 eV),³³ Ag decorated ZnO nanorods (*i.e.* 4.7 eV),¹⁰ and Au faceted oxygen-deficient ZnO nanostructures.²⁴ In the present case, the reduction in work-function is thought to originate from the spitzer shaped truncated tip morphology which might have helped enhance the FE behavior of the ZnO nanowires.

A modified Fowler–Nordheim (F–N) equation (*i.e.* eqn (2)) is used to substantiate the variation in the emission current density of ZnO/ITO emitters subject to the applied field,

$$J = \alpha_f a \Phi^{-1} E^2 \beta_{\text{FE}}^2 \exp\left(-\frac{b \Phi^{3/2}}{\beta_{\text{FE}} E} \nu_F\right) \quad (2)$$

where J is the average FE current density of the device, α_f is a macroscopic pre-exponential correction factor, a and b are constants ($a = 1.54 \times 10^{-6} \text{ A eV V}^{-2}$ and $b = 6.83089 \times 10^3 \text{ eV}^{-3/2} \text{ V } \mu\text{m}^{-1}$), Φ is the work function of the emitter (*i.e.* $\Phi_{\text{ZnO}} = 4.9 \text{ eV}$), E is the average applied electric field, β_{FE} is the local electric field enhancement factor and ν_F is the correction factor also known as the specific value of the principal Schottky–Nordheim barrier function, ν . Due to the random alignment of ZnO nanowires confirmed from FESEM images (Fig. 1), the emission surface of the ZnO/ITO emitters is treated as rough.

Therefore, applied and local electric fields at emission sites (*i.e.* ZnO) differ from each other, and their ratio is identified as β_{FE} . A plot of $\ln\{J/E^2\}$ versus $(1/E)$, accepted as a F–N plot, is illustrated using eqn (2), and the field enhancement factor (β_{FE}) is estimated from equation

$$\beta_{\text{FE}} = \frac{-sb\Phi^{3/2}}{S} \quad (3)$$

where s ($=0.95$), the slope correction factor for the Schottky–Nordheim barrier, is 1 in the present case, for simplicity.

The F–N plots for pristine ZnO/ITO emitters determined at various anode–cathode separations are shown in Fig. 3(c). The distinct F–N plots are ascribed to the well-defined band alignment of the nanowire morphology of ZnO. The optimized



anode–cathode separations in pristine ZnO/ITO emitters have tailored the values of β_{FE} . The β_{FE} values estimated for ZnO/ITO emitters at the anode–cathode separations of 1500, 2000 and 2500 μm are 3089, 3924 and 4760, respectively. These estimated values of β_{FE} for ZnO/ITO emitters are more significant than the reported values of ZnO nanostructure arrays with nanoneedle, nanocavity and bottle shaped morphologies,⁸ hierarchical and pencil-like ZnO nanostructures self-assembled on amorphous carbon,⁹ ZnO branched nanostructures,³⁴ density controlled ZnO nanopillar arrays,¹⁹ tapered ZnO nanorods grown on Fe and Cu electrodes,³⁸ metal doped ZnO nanowires,^{14,15,17} composites of carbon–ZnO,³⁹ and MoS_2/ZnO nano-heterojunctions.⁴⁰ Bae *et al.*²² revealed a field enhancement factor of 2216 for ZnO nanocones, which was not improved after tailoring the density of the nanocones in the emission area. Sugavaneshwar *et al.*³⁴ tailored vapor phase transport to synthesize ZnO nanostructures in the form of wires and branches, but their larger diameter restricted the β_{FE} values in the range of 1129 to 3985. Although Naik *et al.*⁴¹ and Jing *et al.*⁴² have reported larger values of β_{FE} for ZnO nanosheets and nanotowers, respectively, the orthodoxy test known to authenticate such values was not performed to support this. The expediency of the FE measurements and β_{FE} of the ZnO/ITO emitters was confirmed by performing an orthodoxy test utilizing the spreadsheet provided by Forbes in ref. 43. The scaled-barrier-field (f) values estimated for all of the cathode–anode separations in ZnO/ITO emitters are given in Table 1.

The emission situation is orthodox throughout all of the cathode–anode separations of Zn/ITO emitters for the lower (f_{low}) as well as the higher (f_{high}) scaled-barrier-field (f) values. The hexagonal ZnO nanowires with clearly visible textural boundaries revealed reasonable emission behavior for all of the maintained anode–cathode separations. The unique morphological features of the ZnO nanowires, such as hexagonal morphology, individual dispersion, spitzer shaped truncated tips and very sharp pointed tips have resulted in low E_{on} values and large values of β_{FE} for the ZnO/ITO emitters.

This emission behavior can be described in more detail by considering the band alignment of ZnO (Fig. 4(a)). In the present case, owing to unique morphological features, the work function of the ZnO nanowires (*i.e.* 4.9 eV) has been reduced compared to that of reported values (*i.e.* 5.5 to 5.2 eV).^{6–9} The reduced Φ_{ZnO} provides a significantly smaller barrier for the emission of an electron. Therefore, enhancement in FE behavior is expected along with lower E_{on} values and higher values of β_{FE} . In the case of ZnO/ITO emitters, the electrons from the conduction band or its nearest states contribute to

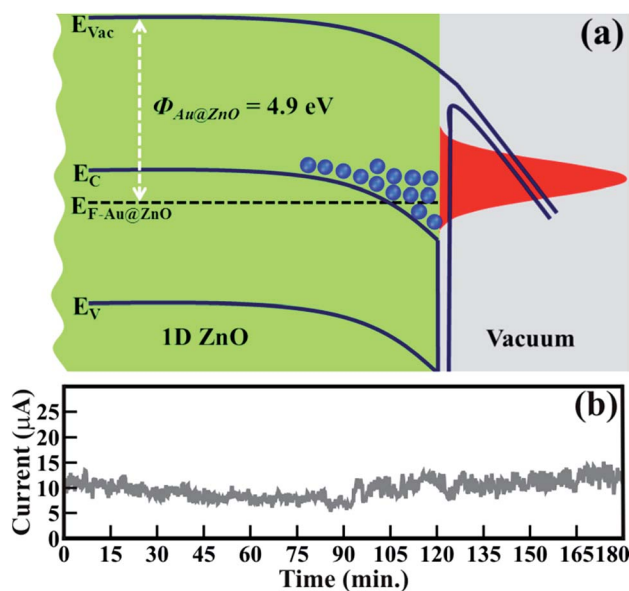


Fig. 4 (a) Schematic band alignment of pristine spitzer shaped ZnO nanowires and (b) field emission current stability ($I-t$) plot of 1D ZnO nanowires.

field emission. Moreover, at an applied electric field, energy band bending generates energy well at a depleted region where a large number of electrons accumulate and are then abruptly emitted in larger quantities due to a relatively lower Φ_{ZnO} (Fig. 4(a)).

Stable field electron emission (*i.e.* current) is one of the prerequisites for utilizing materials for the fabrication of FE displays and related applications. Fig. 4(b) shows the FE stability of ZnO/ITO emitters. The emission current (I) at an applied voltage of 10 μA , assigned as E_{on} , was considered to confirm the stability of ZnO/ITO emitters. A negligible amount of current fluctuation (*i.e.* an average of $\pm 5\%$) was observed even after continuous emission for 180 min. These spitzer shaped 1D ZnO nanowires exhibited very stable and improved electron emission than that of gold nanoparticle decorated ZnO nanopillars,²⁷ monolayer graphene supported by well-aligned ZnO nanowire arrays grown on Si substrates,⁴⁴ seed layer assisted ZnO nanorods,⁴⁵ ZnO nanowires derived after annealing gold deposited Zn substrate at 400 $^{\circ}\text{C}$,⁴⁶ and ZnO multipods, submicron wires and spherical structures obtained by vapour deposition.⁴⁷ The exclusive participation of the sharp tips of the ZnO nanowires as emitters conceivably enhanced the emission ability.

Conclusions

In conclusion, the large area array of stoichiometric and individual dispersed 1D hexagonal ZnO nanowires of spitzer shaped, truncated and very sharp pointed tips synthesized on ITO coated glass substrates resulted in a smaller work-function of 4.9 eV which consequently delivered a significantly smaller E_{on} of $1.56 \text{ V } \mu\text{m}^{-1}$ and stable electron emission (*i.e.* average current fluctuations of $\pm 5\%$). These spitzer shaped ZnO nanowires have

Table 1 Scaled-barrier-field (f) values estimated from F–N plots for ZnO nanowire (*i.e.* ZnO/ITO) emitters using the spreadsheet from ref. 43

Materials	Separation (μm)	f_{low}	f_{high}	Orthodoxy test result
ZnO nanowires	1500	0.29	0.47	Pass
	2000	0.24	0.44	Pass
	2500	0.26	0.50	Pass



potential for utilization in vacuum based micro/nano-devices such as flat-panel displays and intense point electron sources. Moreover, the ZnO nanowires have capabilities to further reduce the work-function and improve electron emission, as well to expand other functionalities for various applications, after the controlled design of nano-hetero-architectures with metals or highly conducting materials.

Conflicts of interest

There are no conflicts to declare.

Acknowledgements

The authors would like to thank the UGC-DAE CSR, Indore, and Department of Science and Technology (DST), Ministry of Science and Technology of India for their financial support of this research under grant No. CSR-IC-BL-65/CRS-182/2017-18/189, and INSPIRE Faculty Award No. DST/INSPIRE Faculty Award/2013/IFA13-PH-63, respectively.

References

- 1 J.-H. Lin, R. A. Patil, M.-A. Wu, L.-G. Yu, K.-D. Liu, W.-T. Gao, R. S. Devan, C.-H. Ho, Y. Liou and Y.-R. Ma, *J. Mater. Chem. C*, 2014, **2**, 8667–8672.
- 2 R. S. Devan, Y. R. Ma, M. A. More, R. T. Khare, V. V. Antad, R. A. Patil, V. P. Thakare, R. S. Dhayal and L. Schmidt-Mende, *RSC Adv.*, 2016, **6**, 98722–98729.
- 3 F. Li, S. M. Wu, L. J. Zhang and Z. Li, *Appl. Phys. A*, 2015, **120**, 1383–1389.
- 4 R. S. Devan, R. A. Patil, J. H. Lin and Y. R. Ma, *Adv. Funct. Mater.*, 2012, **22**, 3326–3370.
- 5 J. H. Lin, R. A. Patil, R. S. Devan, Z. A. Liu, Y. P. Wang, C. H. Ho, Y. Liou and Y. R. Ma, *Sci. Rep.*, 2014, **4**, 6967.
- 6 T. Premkumar, Y. S. Zhou, Y. F. Lu and K. Baskar, *ACS Appl. Mater. Interfaces*, 2010, **2**, 2863–2869.
- 7 F. Yang, W. H. Liu, X. W. Wang, J. Zheng, R. Y. Shi, H. Zhao and H. Q. Yang, *ACS Appl. Mater. Interfaces*, 2012, **4**, 3852–3859.
- 8 Q. Zhao, H. Z. Zhang, Y. W. Zhu, S. Q. Feng, X. C. Sun, J. Xu and D. P. Yu, *Appl. Phys. Lett.*, 2005, **86**, 203115.
- 9 Y. H. Yang, B. Wang, N. S. Xu and G. W. Yang, *Appl. Phys. Lett.*, 2006, **89**, 043108.
- 10 M. J. Li, W. J. Huang, W. J. Qian, B. Y. Liu, H. Lin, W. Li, L. Wan and C. K. Dong, *RSC Adv.*, 2017, **7**, 46760–46766.
- 11 Q. Zhao, J. Y. Gao, R. Zhu, T. C. Cai, S. Wang, X. F. Song, Z. M. Liao, X. H. Chen and D. P. Yu, *Nanotechnology*, 2010, **21**, 095701.
- 12 F. Ye, X. M. Cai, F. P. Dai, S. Y. Jing, D. P. Zhang, P. Fan and L. J. Liu, *Phys. Status Solidi B*, 2012, **249**, 596–599.
- 13 C. X. Xu, X. W. Sun and B. J. Chen, *Appl. Phys. Lett.*, 2004, **84**, 1540–1542.
- 14 C. L. Hsu, C. W. Su and T. J. Hsueh, *RSC Adv.*, 2014, **4**, 2980–2983.
- 15 H. A. Rafaie, R. M. Nor and Y. M. Amin, *Mater. Express*, 2015, **5**, 226–232.
- 16 Z. Zulkifli, G. Kalita and M. Tanemura, *Phys. Status Solidi RRL*, 2015, **9**, 145–148.
- 17 Y. H. Huang, Y. Zhang, Y. S. Gu, X. D. Bai, J. J. Qi, Q. L. Liao and J. Liu, *J. Phys. Chem. C*, 2007, **111**, 9039–9043.
- 18 C. Sun and D. Xue, *J. Phys. Chem. C*, 2013, **117**, 5505–5511.
- 19 Y. M. Chang, J. M. Huang, C. M. Lin, H. Y. Lee, S. Y. Chen and J. Y. Juang, *J. Phys. Chem. C*, 2012, **116**, 8332–8337.
- 20 Z. Zhu, T.-L. Chen, Y. Gu, J. Warren and R. M. Osgood, *Chem. Mater.*, 2005, **17**, 4227–4234.
- 21 P. Nan, X. Haizhou, Y. Minghui, C. Xuefeng, W. Xiaoping, J. G. Hou, H. Jianxing and S. Z. Deng, *Nanotechnology*, 2010, **21**, 225707.
- 22 J. Bae, J. I. Hong, W. H. Han, Y. J. Choi and R. L. Snyder, *Chem. Phys. Lett.*, 2009, **475**, 260–263.
- 23 Q. Zhao, X. Y. Xu, X. F. Song, X. Z. Zhang, D. P. Yu, C. P. Li and L. Guo, *Appl. Phys. Lett.*, 2006, **88**, 033102.
- 24 A. Ghosh, P. Guha, R. Thapa, S. Selvaraj, M. Kumar, B. Rakshit, T. Dash, R. Bar, S. K. Ray and P. V. Satyam, *Nanotechnology*, 2016, **27**, 125701.
- 25 J. H. Lin, Y. J. Huang, Y. P. Su, C. A. Liu, R. S. Devan, C. H. Ho, Y. P. Wang, H. W. Lee, C. M. Chang, Y. Liou and Y. R. Ma, *RSC Adv.*, 2012, **2**, 2123–2127.
- 26 J. F. Moulder, W. F. Stickle, P. E. Sobol and K. D. Bomben, *Handbook of X-ray Photoelectron Spectroscopy*, Perkin-Elmer Corporation, Minnesota, USA, 1992.
- 27 Y. M. Chang, M. L. Lin, T. Y. Lai, H. Y. Lee, C. M. Lin, Y. C. S. Wu and J. Y. Juang, *ACS Appl. Mater. Interfaces*, 2012, **4**, 6676–6682.
- 28 C. H. Ye, Y. Bando, X. S. Fang, G. Z. Shen and D. Golberg, *J. Phys. Chem. C*, 2007, **111**, 12673–12676.
- 29 C. Li, K. Hou, X. X. Yang, K. Qu, W. Lei, X. B. Zhang, B. P. Wang and X. W. Sun, *Appl. Phys. Lett.*, 2008, **93**, 233508.
- 30 R. S. Devan, V. P. Thakare, V. V. Antad, P. R. Chikate, R. T. Khare, M. A. More, R. S. Dhayal, S. I. Patil, Y. R. Ma and L. Schmidt-Mende, *ACS Omega*, 2017, **2**, 2925–2934.
- 31 C. Li, W. Lei, X. B. Zhang, J. X. Wang, X. W. Sun and S. T. Tan, *J. Vac. Sci. Technol., B: Microelectron. Nanometer Struct.–Process., Meas., Phenom.*, 2007, **25**, 590–593.
- 32 J. B. Chen, C. J. Xu, J. C. She, S. Z. Deng, J. Chen and N. S. Xu, *J. Appl. Phys.*, 2010, **107**, 024312.
- 33 J. B. You, X. W. Zhang, P. F. Cai, J. J. Dong, Y. Gao, Z. G. Yin, N. F. Chen, R. Z. Wang and H. Yan, *Appl. Phys. Lett.*, 2009, **94**, 262105.
- 34 R. P. Sugavaneshwar and K. K. Nanda, *Appl. Phys. Lett.*, 2014, **104**, 222104.
- 35 N. S. Liu, G. J. Fang, W. Zeng, H. Long, L. Y. Yuan and X. Z. Zhao, *Appl. Phys. Lett.*, 2009, **95**, 153505.
- 36 B.-A. Fouetio Kengne, S. Karmakar, M. Kaura, V. V. R. Sai, G. Corti, I. B. Niraula, A. Larin, J. Hall, D. Sowell, P. J. Hrdlicka, V. Dobrokhotov and D. N. McIlroy, *ACS Appl. Mater. Interfaces*, 2014, **6**, 13355–13366.
- 37 S. Das, P. Sudhagar, E. Ito, D.-y. Lee, S. Nagarajan, S. Y. Lee, Y. S. Kang and W. Choi, *J. Mater. Chem.*, 2012, **22**, 20490–20497.
- 38 G. Wrobel, M. Piech, P.-X. Gao and S. Dardona, *Cryst. Growth Des.*, 2012, **12**, 5051–5055.



- 39 C. S. Huang, C. Y. Yeh, Y. H. Chang, Y. M. Hsieh, C. Y. Ku and Q. T. Lai, *Diamond Relat. Mater.*, 2009, **18**, 452–456.
- 40 Y.-H. Tan, K. Yu, J.-Z. Li, H. Fu and Z.-Q. Zhu, *J. Appl. Phys.*, 2014, **116**, 064305.
- 41 K. K. Naik, R. Khare, D. Chakravarty, M. A. More, R. Thapa, D. J. Late and C. S. Rout, *Appl. Phys. Lett.*, 2014, **105**, 233101.
- 42 X. Jing, Z. Xianxiang and Z. Gengmin, *Nanotechnology*, 2008, **19**, 295706.
- 43 R. G. Forbes, *Proc. R. Soc. A*, 2013, **469**, 20130271.
- 44 Z. C. Yang, Q. Zhao, Y. G. Ou, W. Wang, H. Li and D. P. Yu, *Appl. Phys. Lett.*, 2012, **101**, 173107.
- 45 Y. F. Liu, C. Li, J. Wang, X. Y. Fan, G. Yuan, S. Xu, M. Xu, J. Zhang and Y. J. Zhao, *Appl. Surf. Sci.*, 2015, **331**, 497–503.
- 46 F. J. Sheinia, D. S. Joag, M. A. More, J. Singh and O. N. Srivasatva, *Mater. Chem. Phys.*, 2010, **120**, 691–696.
- 47 N. S. Ramgir, D. J. Late, A. B. Bhise, M. A. More, I. S. Mulla, D. S. Joag and K. Vijayamohanan, *J. Phys. Chem. B*, 2006, **110**, 18236–18242.

